Journal of Ceramic Processing Research. Vol. 19, No. 3, pp. 272~278 (2018)

J O U R N A L O F
Ceramic Processing Research

Structural evolution of indium hydroxide powders prepared by a precipitation method

Won-Jun Lee[a,b], Eun-Kyoung Choi[a,c], Kyu-Sung Han[a], Jin-Ho Kim[a], Ung-Soo Kim[a], Kwang-Taek Hwang[a], Kwang-Bo Shim[c], Hae-Jin Hwang[b] and Woo-Seok Cho[a,*]

[a]*Icheon Branch, Korea Institute of Ceramic Engineering & Technology, Icheon 17303, Korea*
[b]*School of Material Science and Engineering, Inha University, Incheon 22212, Korea*
[c]*Department of Materials Science and Engineering, Hanyang University, Seoul 04763, Korea*

In this study, we investigated the phase and microstructural changes induced by heat-treatment of indium hydroxide nanoparticles produced by precipitation at various temperatures for different holding times. A white powder was obtained after heating for various times at temperatures of 150-900 ºC. We also investigated changes in the specific surface area of indium oxide prepared by heating the precipitate between 200 and 900 ºC. Finally, we propose a model for the formation of indium oxide powder from the precipitate. The model includes processes such as the formation of bundles of rod-shaped particles, generation of voids in the bundle from the evaporation of crystallized water, strong re-agglomeration of rod-shaped particles, collapse of the rod structure, formation of spherical agglomerates, heterogeneous crystal growth, and homogeneous crystal growth.

Key words: Indium hydroxide, Precipitation method, Transparent conductive oxide, Heat-treatment, Raw material.

Introduction

Indium tin oxide (ITO) is the most widely used transparent conductive oxide due to its high optical transparency in the visible wavelength range, electrical conductivity similar to that of metal, and high reflectance in the infrared region [1]. Indium oxide, an essential starting material used for the preparation of ITO, is an n-type semiconductor oxide and displays a wide band gap of about 3.6 eV at room temperature. In_2O_3 has excellent electrical mobility with a high intrinsic electron concentration. When in the form of very small particles, quantum confinement effects are possible. In addition, it exhibits high electrical conductivity and optical transparency in the visible light region [2].

Recently, In_2O_3 nanoparticles have attracted much attention among researchers for a wide variety of applications in many fields; they can be applied in solar cells [3], field-emission displays [4], lithium-ion batteries [5], nanoscale bio-sensors [6], non-volatile nano-floating gate memory devices [7], gas sensors [8], optoelectronics [9], photocatalysis [10], and field effect transistors [11].

Nano-sized indium oxide can be synthesized by various methods, including sonochemical reaction [12], chemical vapor deposition [13], hydrothermal synthesis [14], and precipitation [15]. Among these, the precipitation method is a relatively simple production process that is cost-effective due to its high yield, and is therefore the most commonly used mass-production method. In this method, indium metal is dissolved in a nitric acid (HNO_3) solution and then neutralized with aqueous ammonia (NH_4OH) or ammonia gas to obtain indium hydroxide powder. The obtained powder is then annealed to yield nano-sized indium oxide powder. In a previous study, we reported the formation mechanism of indium hydroxide considering process parameters such as the pH, concentration, and aging time[16].

In this study, we investigated the phase change and microstructural evolution of indium oxide nanoparticles obtained by heating indium hydroxide using the precipitation method. We studied the effect of processing temperature and time and proposed a model for the formation of the indium oxide powders.

Experimental

Synthesis

For the synthesis of indium hydroxide and indium oxide hydroxide, indium metal (99.99%; Top material) was used as the starting material. First, an aqueous solution of indium nitride was prepared by dissolving indium metal in a nitric acid solution (60% HNO_3, electronic grade; Dongwoo Fine-Chem, Korea) for 2 hrs followed by stirring to obtain a 0.2 M concentration. Then, aqueous ammonia (NH_4OH) was added dropwise to the prepared indium nitride aqueous solution at the

*Corresponding author:
Tel : +82-31-645-1405
Fax: +82-31-645-1486
E-mail: wscho@kicet.re.kr

rate of 3 mL/min to adjust the pH of the solution to 7, forming a white precipitate. The product was collected by centrifugation and then washed. The washed gel-like precipitate was dried at 60 °C using a rotary evaporator (N01200A, EYERA).

In order to investigate the crystallinity and microstructural changes as a function of heating temperature and time, the dried precipitates were heat treated at various temperatures in the range of 150-400 °C for 0-200 hrs (using a drying oven and a furnace). Further, we investigated the changes in the specific surface area of indium oxide prepared by heating the precipitate between 200 and 900 °C.

Characterization

An X-ray diffractometer (XRD; Rigaku, D/2500VL/PC) with a Cu $K\alpha$ ($\lambda = 1.5402$ nm) radiation source was used to determine the crystalline phase and crystallite size of the resulting powder. The crystallite size was calculated using the Scherrer equation:

$$\tau = \frac{K\lambda}{\beta \cos\theta} \quad (1)$$

where β is the full-width-at-half-maximum (FWHM), K is the shape factor, λ is the wavelength (1.54056 Å) and τ is the crystallite size.

Field emission transmission electron microscopy (FE-TEM; JEOL, JEM-2100F) was used to observe the particle morphology. The specific surface area of the obtained powder was estimated using the Brunauer-Emmett-Teller (BET) method using N_2 adsorption isotherms (Micrometrics Tri-Star, Instrument Co., USA).

Results and Discussion

Fig. 1 shows XRD patterns of the powders obtained by heating the dried precipitate in the temperature range of 150-400 °C for 1 hr. The resulting crystalline phases were clearly dependent on the treatment temperature. The $In(OH)_3$ and InOOH phases co-existed in powders annealed at 150 and 200 °C; however, in powders annealed at 250 and 400 °C, $In(OH)_3$ and InOOH had completely reacted to form In_2O_3 phase. This phase transition was presumed to be closely related to the elimination of crystallized water and thermal decomposition of the material.

We investigated the detailed temperature dependence of this degradation reaction on the holding time of heat treatment, which can provide valuable information regarding the synthesis of nano-sized indium oxide powders. Fig. 2 shows the XRD patterns of powders obtained by heat treatment at 150-250 °C for various holding times. $In(OH)_3$ and InOOH phases were observed for the powders annealed at 150 °C for 1-72 hrs, were no dependence on holding time was observed. These results suggest that very little thermal decomposition of the material occurred after the elimination of crystalline water at 150 °C, regardless of

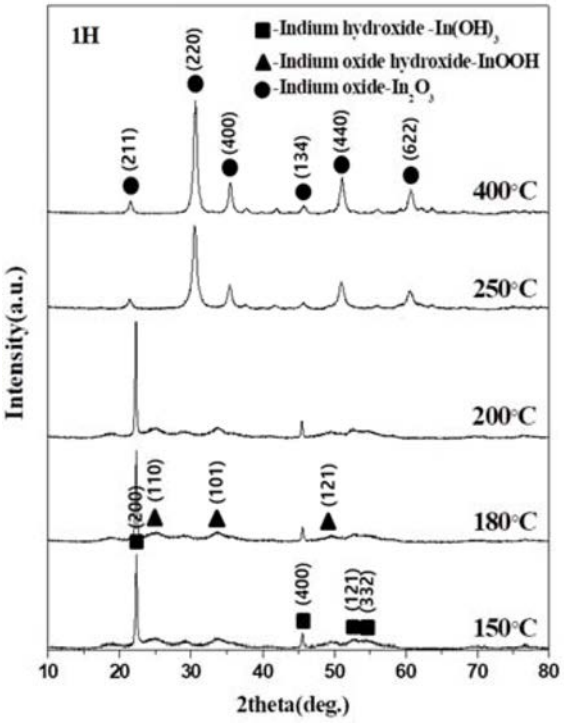

Fig. 1. XRD patterns of the powders obtained from heat treatment of the dried precipitate at various temperatures for 1 hr.

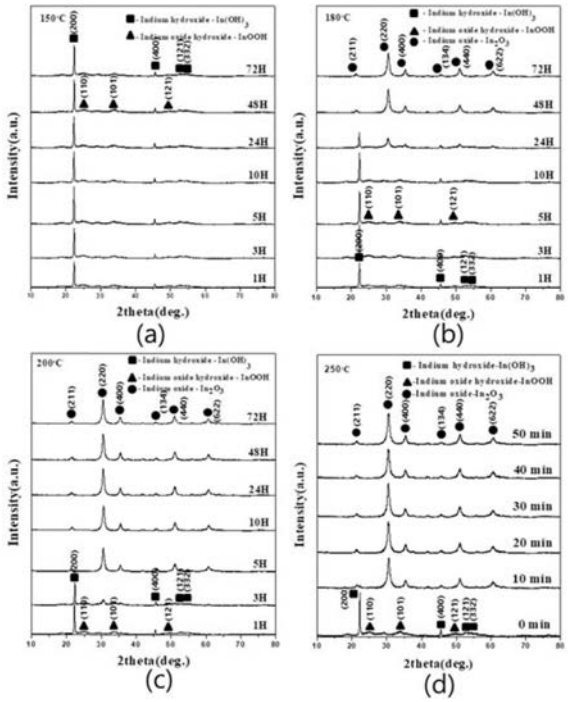

Fig. 2. XRD patterns of the powders obtained by heat treatment for various holding times at temperatures of 150-250 °C.

the holding time. In contrast, for the powder annealed at 250 °C, the phase transition to In_2O_3 occurred immediately above a holding time of 10 min. In the case of powders annealed at 180 and 200 °C, dramatic changes were observed; the $In(OH)_3$ phase rapidly disappears and the amount of the In_2O_3 phase rapidly

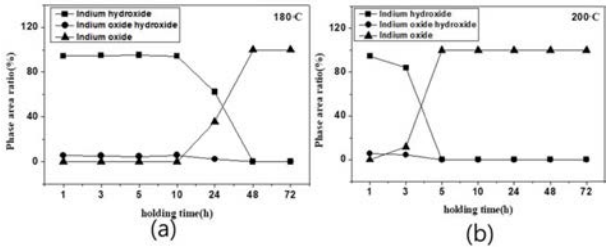

Fig. 3. The integral area ratio of the XRD peaks corresponding to $In(OH)_3$, InOOH, and In_2O_3 with an increase in the holding time at heat treatment temperatures of 180 and 200 °C.

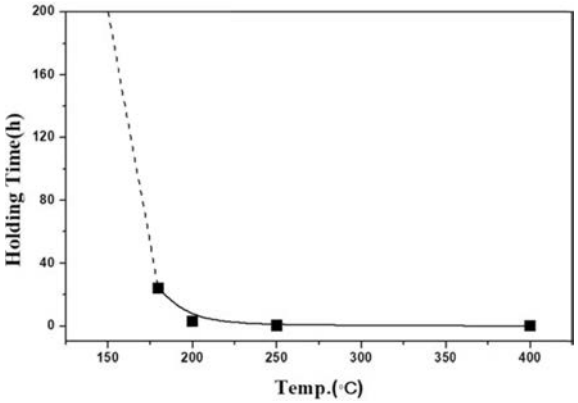

Fig. 4. The holding time at which the phase transition starts to occur rapidly at each temperature.

increases after a certain holding time.

In addition, we systematically investigated how the phase transition to each crystal phase was affected by the holding time at each temperature. Fig. 3 shows the integral area ratio of the XRD peaks corresponding to $In(OH)_3$, InOOH, and In_2O_3 phases with increasing holding time at heat-treatment temperatures of 180 and 200 °C. For the powder annealed at 180 °C for up to 10 hrs, the area ratios of the $In(OH)_3$ and InOOH phases were 95% and 5%, respectively, where no change in the relative percentage with increasing holding time was observed. However, a rapid decrease in the area ratio was observed after 10 hrs. When the heating time reached 24 hrs, the area ratios of $In(OH)_3$ and InOOH decreased to 62.3% and 2%, respectively, and the newly formed In_2O_3 phase was observed, with a ratio of ~33% (Fig. 3(a)). The area ratios of $In(OH)_3$ and InOOH were 95% and 5%, respectively, after heating at 200 °C for 1 hr. With an increase in the holding time to 3 hes, all three phases co-existed; the area ratio of the $In(OH)_3$ phase was ~84%, whereas those of the InOOH and In_2O_3 phases were ~4% and 12%, respectively. For powders annealed for more than 5 hrs, the crystalline phase underwent complete transition to In_2O_3 (Fig. 3(b)).

The change in the area ratio between these crystal phases was categorized into three stages, where the phase transition from $In(OH)_3$ to In_2O_3 was clearly observed. In the first stage, there was little change with increasing holding time. As shown in Fig. 3, the duration of this first stage became shorter as the heating temperature was increased. In the second stage, dramatic phase transitions occurred with acceleration of these changes with increasing temperature. In the third stage, the phase transition had terminated and the final In_2O_3 content was stable. It was also found that the third stage was initiated sooner at higher temperature. The phase transition behavior from InOOH to In_2O_3 showed a similar trend as that for the $In(OH)_3$ phase. However, since the amount of InOOH phase produced was very small, this change was not clearly observed. These results show that the phase transition of interest was closely related to the thermal decomposition of crystal water.

Fig. 4 shows the time at which the rapid phase transition occurred as a function of heat-treatment temperature. In the case of heat treatment at 150 °C, the phase transition to indium oxide did not occurr until after 168 hrs, while this time rapidly decreased to 24 hrs at 180 °C, 3 hrs at 200 °C, and 10 min at 250 °C; no holding time was required at 400 °C. The rate of phase transition at different heating temperatures was due the thermal decomposition of crystal water and is highly dependent on temperature. Fig. 4 shows that the relationship between the heat-treatment temperature and the onset time of phase transition was exponential.

In general, the activation energy of a reaction is temperature dependent, and the phase transition rate can be dramatically increased by increasing the heating temperature. However, changes in temperature and time do not only affect the phase transition rate; they are often accompanied by changes in the crystallinity and particle size. Therefore, many powder properties need to simultaneously be characterized to understand the overall effect of changing the temperature to control the phase transition rate. The crystallite size of each phase was calculated using the Scherrer equation using the main peaks at $2\theta = 22.2°$, 25.8 °, and 30.5 ° corresponding to the $In(OH)_3$, InOOH, and In_2O_3 phases, respectively, from the XRD patterns in Fig. 5. No change in the crystallite size was observed for the powders heat treated at 150 °C for various holding times. The crystallite size of the $In(OH)_3$ phase was approximately 34-38 nm and that of the InOOH phase was 4-6 nm (Fig. 5(a)). In the case of the powder annealed at 180 °C, the crystallite size of the $In(OH)_3$ phase was ~36-38 nm, that of the InOOH phase was ~5-6 nm, and that of the In_2O_3 phase formed after 24 hrs holding time was 12-14 nm (Fig. 5(b)). The crystallite size of the In_2O_3 powders obtained from heat treatment at 200 °C and 400 °C was 13-16 nm (Figs. 5(c) and 5(d)). Hence, we conclude that, at the conditions used in this study, changes in the phase transition rates were not accompanied by changes in the crystallite size.

Fig. 6 shows the specific surface areas of the

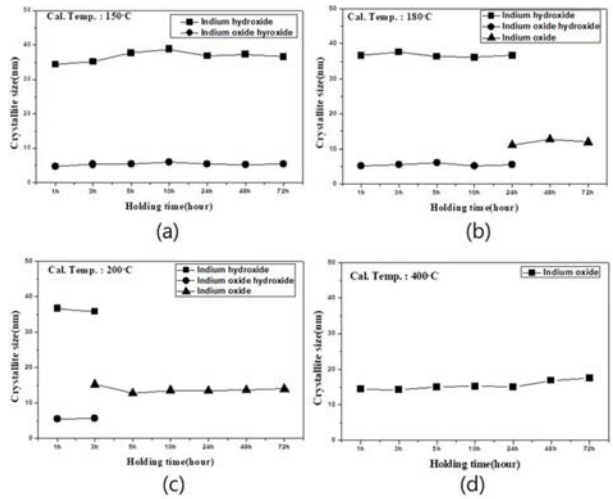

Fig. 5. Change in the crystallite sizes of indium hydroxide, indium oxide hydroxide, and indium oxide determined using the Scherrer equation for the powders heat treated at various temperatures.

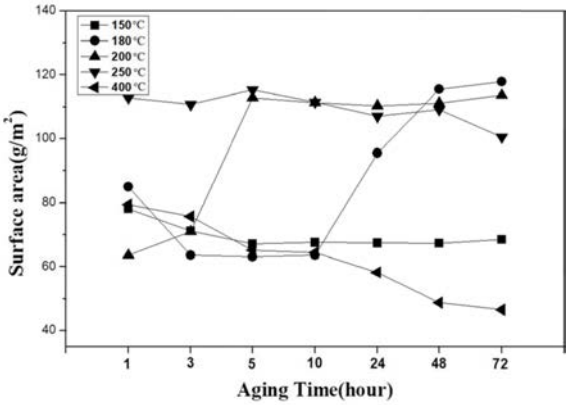

Fig. 6. BET specific surface areas of powders obtained by heat treatment at various temperatures and holding times.

powders obtained by varying the heating temperatures and holding times. The specific surface area was 78.03 g/m^2 for the powder annealed at 150 ºC for 1 hr, which slightly decreased to 71.12 g/m^2 after 3 hrs, and then remained almost constant at 68 g/m^2 after 5 hrs. However, at 180 ºC, the specific surface area was 84.9 g/m^2 after 1 hr, which then decreased to 63.6 g/m^2 after 3 hrs, and increased thereafter by ~50 g/m^2 to 114 g/m^2 after 24 hrs. For the powder annealed at 200 ºC, the specific surface area was 63.6 g/m^2 after 1 hr, which subsequently increased by ~49 g/m^2 to 112.8 g/m^2 after 5 hrs. These trends in the onset time of the increase in the specific surface area and the time to reach the maximum value were similar to those for the phase transition observed from the XRD results. Thus, we can speculate that the change in the specific surface area was directly related to the phase transition.

However, in contrast, the crystallite size did not change noticeably with increasing heating temperature and holding time. Thus, the changes in the crystallite size and particle size followed different trends depending on the heat treatment condition. To confirm this phenomenon, TEM images of the powders treated at 180 ºC for 10 and 72 hrs were obtained (Fig. 7). As shown in Fig. 3 and Fig. 6, these two samples clearly demonstrate the correlation between the change in the specific surface area and the phase transition of $In(OH)_3$ to In_2O_3 with increasing heating time. In a previous study, we found that $In(OH)_3$ aggregates into bundles of rod-shaped particles [16]. During the heat treatment process, crystal water within these bundle-like secondary particles is removed. This in turn could cause the rod-shaped particles to shrink, resulting in a volume reduction and increase in the void space in the bundle. The increasing area of the brighter features in the TEM image is thought to correspond to this increase in void space volume. Furthermore, with increasing holding time, no increase in the crystallite sizes of the $In(OH)_3$ and In_2O_3 phases was observed. However, as shown in Fig.

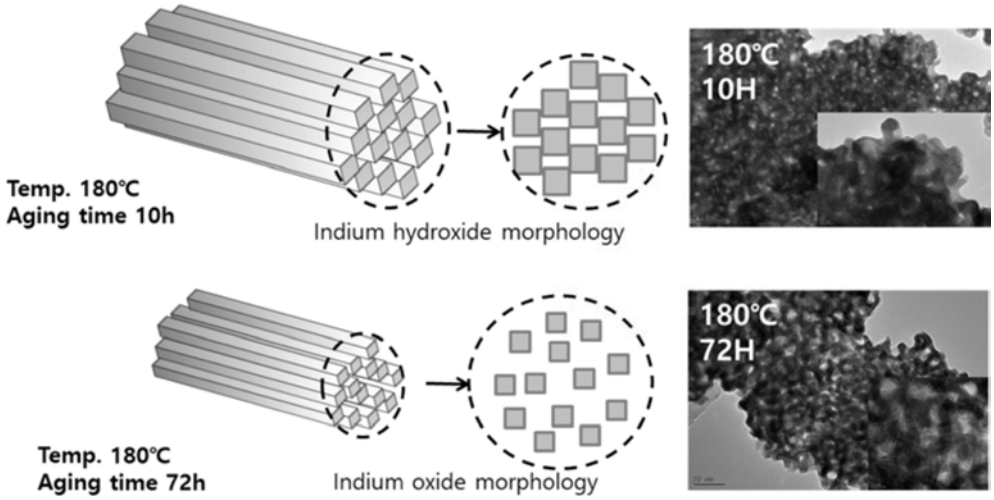

Fig. 7. TEM micrographs and schematic illustrations of indium hydroxide powders heat treated at 180 ºC for 10 hrs and 72 hrs.

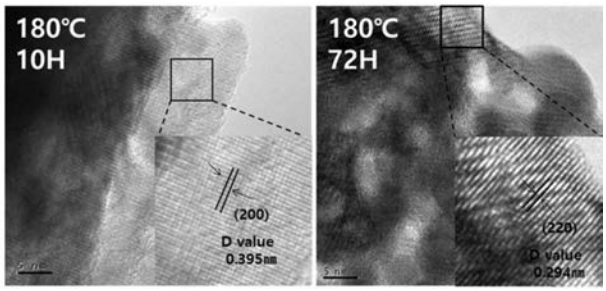

Fig. 8. TEM micrographs of indium hydroxide powders heated at 180 ºC for 10 hrs and 72 hrs.

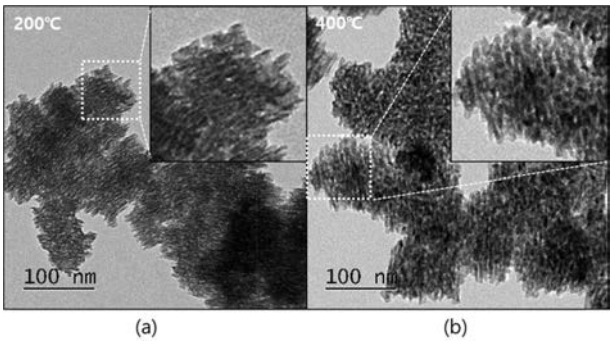

Fig. 10. TEM micrographs of indium hydroxide heated at (a) 200 and 400 ºC.

8, a surface area of 3.95 Å corresponding to the *d* spacing of the indium hydroxide lattice was observed for the sample annealed at 180 ºC for 10 hrs, while a surface area of 2.94 Å corresponding to the *d* value characteristic of indium oxide was observed for the sample annealed for 72 hrs. Hence, we conclude that the transition from the $In(OH)_3$ phase to the In_2O_3 phase occurred due to the degradation of crystal water and, although the crystallite size did not change during this process, voids within the bundles became larger and the specific surface area increased due to contraction of the rod-shaped particles.

To observe the growth behavior of indium oxide particles as a function of heating temperature, TEM images of indium hydroxide powders annealed at various temperatures are shown in Fig. 9. The powder obtained by heating at 200 ºC comprised bundles of rod-shaped particles. At temperatures of 300-400 ºC, the particles increased in size owing to the aggregation of the rod-shaped bundles which had a high surface energy. In the range of 600-900 ºC, crystal growth of spherical particles was observed. We focused on the point at which the rod-shaped bundles transformed into aggregated spherical particles. Fig. 10 shows a TEM image of the powder obtained by heating at 200 ºC, which exhibits bundles of rod-shaped particles, along with a TEM image of the powder obtained by heating at 400 ºC, which shows this shape transformation. Unlike the powder annealed at 200 ºC, that annealed at 400 ºC showed that the bundled rod-like particles disintegrated into much smaller spherical particles (~5 nm); these appeared like rods on the macroscopic scale (Fig. 10(b)). It is thought that this phenomenon provided a driving force for the rod-shaped particles to transform into spherical ones, which progresses with the crystal growth into a spherical one. Hence, the small spherical particles grew to ~10 nm at 600 ºC, and a polydisperse size distribution with particle sizes of 10-50 nm was observed at 700 ºC. This may have been

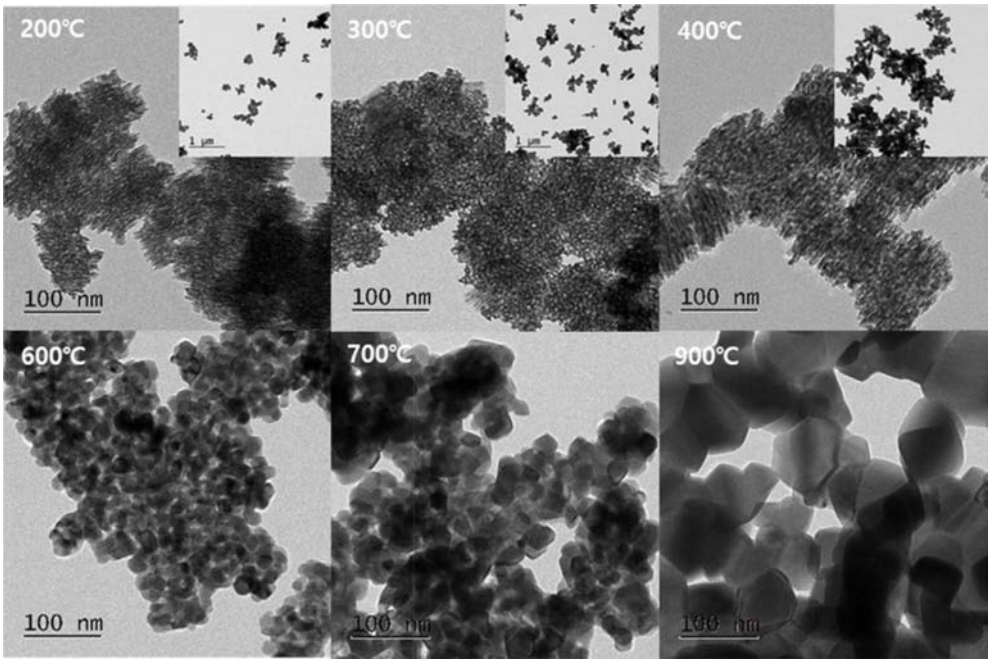

Fig. 9. TEM micrographs of indium hydroxide heated at various temperatures.

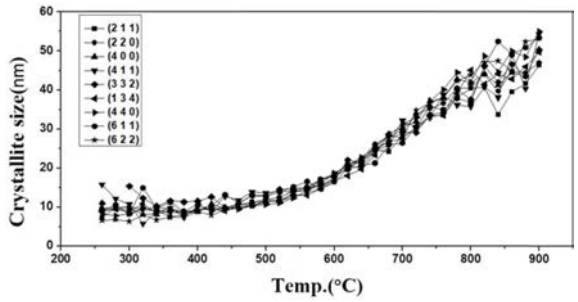

Fig. 11. The crystallite sizes for various crystal directions of the powders obtained by heat treatment at various temperatures.

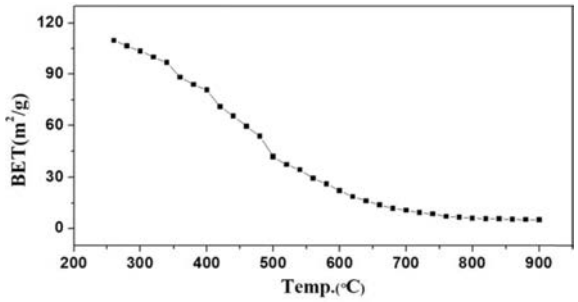

Fig. 12. BET specific surface areas of powders obtained by heating at various temperatures.

due to the local aggregation and differences in the surface energies of the particles, resulting in different crystal growth environments. However, at 900 °C, the particles grew up to 50-60 nm and gradually become less sensitive to the differences in the local environmental factors, finally resulting in the formation of powders with a relatively uniform particle distribution.

Next, we investigated variations in the crystallite size and specific surface area as a function of the heating temperature. This was due to the unusual behaviors observed below 200 °C, contrary to the expected behavior. Fig. 11 shows the calculated crystallite sizes of powders annealed at varying temperatures up to 900 °C obtained from XRD data. Between 260 and 500 °C, the size of the crystallites was ~10 nm and the size gradually increased with further temperature increases. In addition, for powders annealed above 600 °C, a rapid increase in the crystallite size was observed. Considering Fig. 9 and Fig. 11, we concluded the following three factors. First, each particle was a single crystal, supported by the observation that the individual particle sizes in the TEM images of powders annealed at 600, 700, and 900 °C (Fig. 9) were the same as the crystallite sizes observed from Fig. 11. Second, since the crystallite sizes from all crystal directions were similar, isotropic crystal growth occurred without any preferred growth orientation. Lastly, a high temperature above 600 °C was necessary for rapid crystal growth.

Fig. 12 shows the specific surface areas of powders annealed at 260-900 °C. Between 260 and 600 °C, a rapid decrease in the surface area was observed, with the rate of decrease slowing above 600 °C. We attribute this to the specific surface area dramatically decreasing owing to the rapid and strong aggregation of fine particles up to 600 °C, rather than crystal growth caused by the increased temperature. For temperatures above 600 °C, the specific surface area steadily decreased due to crystal growth rather than the strong aggregation.

Conclusions

In this study, the precipitate of indium hydroxide was obtained by dissolving indium metal in a solution of nitric acid, followed by the addition of aqueous ammonia to neutralize the pH. The obtained precipitate was subsequently heated at various temperatures for different holding times and changes in the crystal phase and microstructural evolution were evaluated.

We proposed a model for the phase transformation from the indium hydroxide obtained by the precipitation method to indium oxide and the growth of nanocrystals. The precipitate is usually obtained in the form of indium hydroxide comprised of rod-shaped bundles. With increasing temperature, gradual thermal decomposition resulted in phase transformation from indium hydroxide to indium oxide occurring. The kinetics of the phase

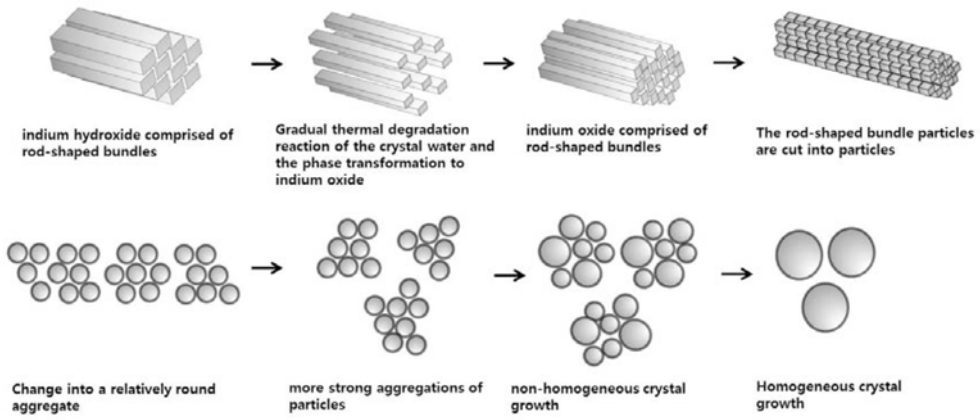

Fig. 13. Schematic illustration of the crystal growth mechanism of indium hydroxide.

transformation increased exponentially with increasing heat-treatment temperature. In addition, during phase transformation, there was a decrease in the particle volume due to the thermal degradation of crystal water and subsequent formation of temporary void spaces within the rod-shaped bundles, resulting in an increase in the specific surface area. When the holding time was extended or the temperature increased, the specific surface area decreased due to higher aggregation forces and the voids disappeared. When the temperature was increased to ~400 °C, the rod-shaped bundles disintegrated into spherical particles with a much smaller size of ~5 nm, which were not distinctly separate and thus, appeared macroscopically as rods. The particles aggregated more strongly up to 600 °C, leading to a rapid decrease in the specific surface area, with no noticeable crystal growth. Additionally, as the rod-shaped particles partially disintegrated, they changed into spherical aggregates. Above 600 °C, relatively rapid crystal growth occurs. Initially, an irregular particle size distribution was observed which became relatively uniform when the heat-treatment temperature increased to 900 °C.

We elucidated the process of crystal growth from the precipitate and our findings are expected to provide very important insights into controlling the shape and characteristics of such particles. In addition, we believe that the results of this study can aid in improving the sintering properties of the sputtering target used to fabricate transparent electrodes and ultimately contribute to improving the properties and productivity of transparent electrodes.

Acknowledgments

This work was supported by the Infrastructure Program for New Value Creation of Traditional Ceramic Industry (18-BUS010025000) under the Ministry of Trade, Industry, and Energy, Korea.

References

1. K. Utsumi, H. Ligusa, R. Tokumaru, P.K. Song and Y. Shigesato, Thin Solid Films 445 (2003) 229.
2. N. Donato, F. Neri, G. Neri, M. Latino, F. Barreca, S. Spadaro, I. Pisagatti, and G. Curro, Thin Solid Films 520[3] (2011) 922-926.
3. Z. B. Zhou, R. Q. Cui, Q. J. Pang, Y. D. Wang, F. Y. Meng, T. T. Sun, Z. M. Ding, and X. B. Yu, Appl. Surf. Sci. 172[3] (2001) 245-252.
4. Y. X. Liang, S. Q. Li, L. Nie, Y. G. Wang, and T. H. Wang, Appl. Phys. Lett. 88 (2006) 193119.
5. D. W. Kim, I. S. Hwang, S. J. Kwon, H. Y. Kang, K. S. Park, Y. J. Choi, K. Choi, and J. G. Park, Nano Lett. 7[10] (2007) 3041-3045.
6. M. Curreli, C. Li, Y. Sun, B. Lei, M. A. Gundersen, M. E. Thompson, and C. Zhou, J. Am. Chem. Soc. 127[19] (2005) 6922-6923.
7. S. P. Kim, T. H. Lee, D. U. Lee, E. K. Kim, H. M. Koo, W. J. Cho, and Y. H. Kim, Curr. Appl. Phys. 9[1] (2009) S43-S46.
8. S. Z. Huang, W. Lin, and W. Z. Chen, Trans. Nonferrous Met. Soc. China 19[1] (2009) s80-s82.
9. G. Golan, A. Axelevitch, B. Gorenstein, and A. Peled, Appl. Surf. Sci. 253[15] (2007) 6608-6611.
10. B. Li, Y. Xie, M. Jing, G. Rong, Y. Tang, and G. Zhang, Langmuir 22[22] (2006) 9380-9385.
11. C. Li, D. Zhang, S. Han, T. Tang, J. Hen, W. Jin, and C. Zhou, Appl. Phys. Lett. 82 (2003) 1613.
12. M. S. Y. Parast and A. Morsali, Ultrason. Sonochem. 18[1] (2011) 375-381.
13. J. S. Jeong, J. Y. Lee, C. J. Lee, S. J. An, and G. C. Yi, Chem. Phys. Lett. 384[4] (2004) 246-250.
14. T. T. Tseng and W. J. Tseng, Ceram. Int. 35[7] (2009) 2837-2844.
15. Y. Luo, X. Zheng, L. Zou, S. Hu, and J. Yang, ECS Solid State Lett. 4[7] (2015) 2162-8742.
16. W. J. Lee, U. K. Choi, U. S. Kim, J. Y. Kim, K. B. Sim, H. J. Hwang, and W. S. Cho, J. Ceram. Proc. Res. 18[11] (2017) 805-809.